Mon. Not. R. Astron. Soc. **374,** 1473–1478 (2007) doi:10.1111/j.1365-2966.2006.11249.x

The *Swift* gamma-ray burst GRB 050422

A. P. Beardmore,[1⋆] K. L. Page,[1] P. T. O'Brien,[1] J. P. Osborne,[1] S. Kobayashi,[2] B. Zhang,[3] D. N. Burrows,[4] M. Capalbi,[5] M. R. Goad,[1] O. Godet,[1] J. E. Hill,[6,7] V. La Parola,[8] F. Marshall[6] and A. A. Wells[1]

[1]*Department of Physics and Astronomy, University of Leicester, Leicester LE1 7RH*
[2]*Astrophysics Research Institute, Liverpool John Moores University, Birkenhead CH41 1LD*
[3]*Physics Department, University of Nevada, Las Vegas, NV, USA*
[4]*Department of Astronomy & Astrophysics, 517 Davey Lab, Pennsylvania State University, University Park, PA 16802, USA*
[5]*ASI Science Data Centre, via Galileo Galilei, 00044 Frascati, Italy*
[6]*NASA/Goddard Space Flight Center, Greenbelt, MD 20771, USA*
[7]*Universities Space Research Association, 10211 Wincopin Circle, Suite 500, Columbia, MD, 21044, USA*
[8]*INAF – Istituto di Astrofisica Spaziale e Fisica Cosmica di Palermo, Via Ugo La Malfa 153, 90146 Palermo, Italy*

Accepted 2006 November 3. Received 2006 September 15; in original form 2006 February 15

ABSTRACT

We describe observations of GRB 050422, a *Swift*-discovered gamma-ray burst. The prompt gamma-ray emission had a T_{90} duration of 59 s and was multipeaked, with the main peak occurring at $T + 53$ s. *Swift* was able to follow the X-ray afterglow within 100 s of the burst trigger. The X-ray light curve, which shows a steep early decline, can be described by a broken power law with an initial decay slope of $\alpha_1 \sim 5.0$, a break time $t_b \sim 270$ s and a post-break decay slope of $\alpha_2 \sim 0.9$, when the zero time of the X-ray emission is taken to be the burst trigger time. However, if the zero time is shifted to coincide with the onset of main peak in the gamma-ray light curve then the initial decay slope is shallower with $\alpha_1 \sim 3.2$. The initial gamma-ray spectrum can be modelled by a power law with a spectral index of $\beta_B = 0.50 \pm 0.19$. However, the early time X-ray spectrum is significantly steeper than this and requires a spectral index of $\beta_X = 2.33^{+0.58}_{-0.55}$.

In comparison with other *Swift* bursts, GRB 050422 was unusually X-ray faint, had a soft X-ray spectrum, and had an unusually steep early X-ray decline. Even so, its behaviour can be accommodated by standard models. The combined BAT/XRT light curve indicates that the initial, steeply declining, X-ray emission is related to the tail of the prompt gamma-ray emission. The shallower decay seen after the break is consistent with the standard afterglow model.

Key words: gamma-rays: bursts.

1 INTRODUCTION

Gamma-ray bursts (GRBs) are highly energetic, short-lived phenomena. A long burst, like the one considered here, has a typical prompt gamma-ray emission duration of 10–100 s, during which time $\sim 10^{51}$ erg of energy are released (Frail et al. 2001; Bloom, Frail & Kulkarni 2003). The favoured theoretical explanation for long bursts is the collapsar model (Woosley 1993). In this scenario, the core collapse of a rapidly rotating massive star generates ultrarelativistic outflows (bulk Lorentz factor $\Gamma \sim 100$), in the form of two opposing collimated outflows (MacFadyen & Woosley 1999; Zhang, Woosley & Heger 2004). The initial gamma-ray flux is thought to arise from synchrotron emission when electrons are accelerated to near light speed by internal shocks, which form when the Lorentz factor of the outflowing material is variable (Rees & Mészáros 1994). Observational evidence linking the collapsar model with long GRBs was obtained with the discovery of a type Ic supernova, SN 2003dh, associated with GRB 030329 (Hjorth et al. 2003; Stanek et al. 2003). In addition to the prompt gamma-ray emission, the outflowing material eventually collides with the surrounding interstellar medium (ISM), or previously ejected stellar material, and causes an external shock, which gives rise to afterglow emission from the X-ray to radio bands (Mészáros & Rees 1997). A full review of GRB properties and models prior to the launch of *Swift* can be found in Zhang & Mészáros (2004).

Until recently, it has proven difficult to obtain X-ray afterglow data in a timely fashion after the burst. For example, *BeppoSAX*

⋆E-mail: apb@star.le.ac.uk

only routinely followed bursts with its narrow field instruments ∼8 h after the initial burst trigger (Frontera 2003; Piro 2004), and, therefore, missed out on the study of early afterglow data, which is crucial in order to provide a full understanding of the physics of the outflow, and the engine behind it. It left unanswered questions such as: how are the prompt and later time afterglow emission related? Are they both formed in the external shock, or does the prompt emission come from internal shocks and the afterglow emission from external shocks? The *Swift* Gamma-Ray Explorer (Gehrels et al. 2004) was launched on 2004 November 20 with the main mission objectives of discovering new GRBs, rapidly localizing their positions for subsequent follow-up observations and making extended observations of the associated afterglows. In doing so, it fills the data gap at early times. *Swift* achieves this goal by detecting transient gamma-ray emission with the Burst Alert Telescope (BAT). It then rapidly manoeuvres to point two narrow field telescopes, the X-ray Telescope (XRT), and the UltraViolet/Optical Telescope (UVOT), at the newly discovered burst. The three instruments are described in Barthelmy et al. (2005), Burrows et al. (2005a) and Roming et al. (2005), respectively. The BAT covers the energy range 15–350 keV with an imaging capability of a few arcminutes, while the XRT is sensitive in the 0.2–10.0 keV band with a ∼5 arcsec positional accuracy. The UVOT is capable of subarcsecond positional accuracy and has three broad-band visual filters (corresponding to the U, B and V bands), three broad-band UV filters, a white light filter and UV/optical grisms.

Swift has discovered GRBs at a rate of ∼100 per year. Results so far include: steep early decays seen in the X-ray light curves, often lasting a few hundred seconds, which appear to be associated with the fading, prompt gamma-ray emission (Tagliaferri et al. 2005; Cusumano et al. 2006; Goad et al. 2006; Nousek et al. 2006; O'Brien et al. 2006; Vaughan et al. 2006), these are usually followed by a transition to a flatter light curve, with an additional break at later times; the presence of large flares in about 30 per cent of bursts, which appear minutes to hours after the initial trigger, the largest example of which released as much energy as the prompt emission itself (Burrows et al. 2005b; Falcone et al. 2006; Romano et al. 2006).

This paper reports the *Swift*-detected burst GRB 050422 and its afterglow, the X-ray spectrum and light curve of which are unusually steep.

2 OBSERVATIONS AND ANALYSIS

The *Swift* BAT triggered on GRB 050422 (trigger number 115214) on 2005 April 22 at 07:52:39.8 UT (Barbier et al. 2006). The ground-processed BAT position was RA (J2000) = $21^{\rm h}37^{\rm m}49^{\rm s}$, Dec. (J2000) = $+55^\circ47'53''$, with a 3-arcmin uncertainty (Suzuki et al. 2005). *Swift* slewed immediately towards the BAT position and the XRT began settling on to the burst in Low-rate Photodiode Mode (LrPD), 100 s after the BAT trigger. Eight seconds later, once settling was complete, the XRT initiated its automated response to a new GRB and started taking data in image mode (IM), followed by piled-up photodiode mode (PuPD), LrPD mode, windowed timing (WT) mode and photon counting (PC) mode, where the latter modes depend on the source flux. [A full description of the XRT operating modes can be found in Hill et al. (2004).] The exposure time for the first orbit was 545 s.

Unfortunately, because of the faint nature of the burst, together with a cosmic ray event which struck the CCD detector almost head on, the XRT's onboard software did not centroid on a valid source in the IM data. However, once the first PC mode data were available for ground processing, an uncatalogued X-ray source was found at RA (J2000) = $21^{\rm h}37^{\rm m}54\overset{\rm s}{.}9$, Dec. (J2000) = $+55^\circ46'\,45\overset{''}{.}3$, with an uncertainty of 3.6 arcsec. This position uses the latest XRT boresight correction (Moretti et al. 2005). The X-ray source was found to be rapidly decaying in intensity, making it undoubtedly the counterpart to the gamma-ray burst.

The UVOT observation began 112 s after the BAT trigger with a 100-s V-band finding chart exposure. This revealed no new optical source at the location of the GRB. The UVOT then followed its usual automated response to a new GRB by cycling through its filters in a pre-defined sequence.

The following sections describe the *Swift* observations in more detail. We characterize the flux as a function of time, t and frequency, ν, with functions of the form $F(t,\,\nu) \propto (t - t_0)^{-\alpha}\nu^{-\beta}$, where α is the temporal decay index, t_0 is the decay zero time and β is the spectral energy index (related to the photon index, $\Gamma_{\rm p}$, by $\beta = \Gamma_{\rm p} - 1$). The data analysis was performed using release 2.0 of the *Swift* software tools. Parameter uncertainties are estimated at the 90 per cent confidence level.

2.1 Gamma-ray

Fig. 1 shows the BAT light curve obtained after ground processing of the data. The light curves are displayed in the standard BAT energy bands of 15–25, 25–50, 50–100 and 100–350 keV and are plotted with respect to the BAT trigger time (T). The burst had a T_{90} duration of 59.2 ± 0.5 s and shows a multipeaked light curve which is most prominent below 100 keV. The main peak occurs at $T + 52.8 \pm 0.7$ s, with a full width at half-maximum of 10.8 ± 1.5 s, suggesting the gamma-ray burst central engine was reinvigorated a short time after the initial trigger.

The BAT spectrum for the duration of the burst is shown in Fig. 2. A simple power-law model gave an acceptable fit, with an energy index $\beta_{\rm B} = 0.50 \pm 0.19$ ($\chi^2/\nu = 36.6/57$). The observed flux for this spectrum was 1.0×10^{-8} erg cm^{-2} s^{-1} over the energy range 15–150 keV, corresponding to a fluence of 5.9×10^{-7} erg cm^{-2}, which is a factor of 2 below the average for BAT-detected bursts (O'Brien et al. 2006).

A cut-off power-law model was also tried but did not improve the fit, resulting in an unconstrained high-energy cut-off.

In order to search for any spectral evolution, the data were divided into two at $T + 43$ s, which covers the time period up to the start of

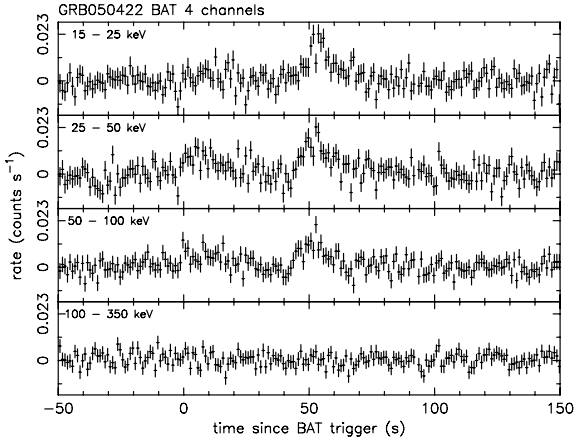

Figure 1. The BAT energy resolved light curve for GRB 050422 plotted relative to the trigger time derived from ground processing. The energy bands are, from top to bottom, 15–25, 25–50, 50–100 and 100–350 keV.

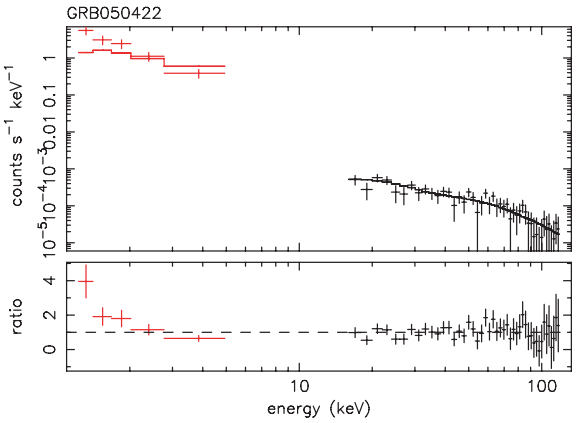

Figure 2. The BAT and the early-time XRT WT spectra of GRB 050422 modelled with a simple absorbed power law. The joint spectral fit was made using the spectral index found for the BAT data alone, while the normalizations were left free to account for the non-simultaneous nature of the observations. The fit and residuals illustrate that the spectrum observed by the XRT is significantly softer.

the main peak and the main peak itself. Spectral indices of 0.30 ± 0.38 and 0.82 ± 0.21 were found for the pre-peak data and during the main peak, respectively. While the measured values are within the formal errors there is a suggestion that the BAT spectrum becomes softer at later times, which is borne out by the early time XRT observation (see Section 2.2.2, below).

2.2 X-ray

GRB 050422 was initially observed as an automated XRT target until a nominal 60-ks exposure had elapsed, at which point it was reintroduced into the *Swift* observing schedule as a pre-planned science target. In total, the XRT observations spanned 17.6 d in 10 separate observing segments with an on-source time of 289 ks. Table 1 shows the XRT observation log.

2.2.1 Temporal analysis

An X-ray light curve was created with data from LrPD mode (including when the observatory was in the latter stages of slewing and settling), PuPD mode, WT mode and PC mode. Event grades 0–5 (LrPD), 0–2 (WT) and 0–12 (PC) were considered (i.e. up to four pixels in size), in order to maximize the CCD quantum efficiency at higher energies. The data from the WT and PC modes were background subtracted using simultaneous off source regions, whereas the LrPD and PuPD data had a constant value subtracted which was estimated from the early and late slew data.

Table 1. *Swift* XRT observation log for GRB 050422.

Segment[a]	Mode	Start[b]	Stop[b]	Exposure[c]	Comment
00	LrPD	97.5 s	99.5 s	2.0 s	Slew data
00	LrPD	100.2 s	108.2 s	8.0 s	Settling data
00	IM	109.5 s	109.6 s	0.1 s	Terminated by Cosmic ray
00	PuPD	112.3 s	113.3 s	1.0 s	
00	LrPD	113.6 s	114.6 s	1.0 s	
00	WT	115.1 s	133.1 s	18.0 s	
00	PC	134.4 s	145.2 ks	56.6 ks	
01–02	PC	148.6 ks	445.2 ks	77.3 ks	
03–05	PC	490.3 ks	919.0 ks	77.2 ks	
06–10	PC	924.8 ks	1522.3 ks	77.9 ks	XRT upper limit only

[a]Corresponds to the last two digits of the observation identification number (001152140xx); [b]seconds (s) or kiloseconds (ks) from the BAT trigger at 2005 April 22 07:52:39.8 UT; [c]seconds (s) or kiloseconds (ks).

PC mode data are susceptible to the effects of pile-up in the core of the XRT's point spread function (PSF) when the count rate exceeds $\sim$0.7 counts s^{-1} (Vaughan et al. 2006; Moretti, private communication). To investigate the effects of pile-up for this target, the radial intensity profile of the source was computed for data from the first orbit and compared to the expected PSF profile for a non-piled-up source from ground calibration data (Moretti et al. 2004). This revealed a deficit of counts within a three-pixel central radius, suggestive of pile-up. The data for this period were, therefore, extracted from an annular region which excluded the three inner-most radial pixels, and then adjusted for the loss of the central part of the PSF (by a factor of 2.26), to give a pile-up-corrected light curve. The PC data at later times (beyond $T + 200$ s) were not bright enough to suffer from pile-up-related problems.

The 0.3–10.0 keV light curve for the entire XRT observation of GRB 050422 is shown in Fig. 3, again plotted with respect to the BAT trigger time. The data have been binned to have a minimum of 20 counts bin^{-1} to satisfy the requirements for χ^2 fitting. This means at later times many orbits of data were summed together in order to reach the required significance level. The last point, however, is only a 2.2σ detection (at 14 background-subtracted source counts in an exposure of 78 ks), and is plotted as an upper limit.

The light curve shows a steep early decline and then flattens off at later times. Formally, fitting a single power-law decay slope to the data gives a poor fit ($\chi^2/\nu = 68.5/20$). However, fitting a broken power law to the data gives a excellent fit ($\chi^2/\nu = 17.0/18$), with a steep pre-break decay slope of $\alpha_1 = 4.97^{+0.53}_{-0.37}$, a break time $t_b = 272^{+43}_{-25}$ s, and a post-break slope of $\alpha_2 = 0.92^{+0.13}_{-0.16}$.

We note that the light curve appears to level off at later times ($T > 10^5$ s). The low Galactic latitude of the burst places it in a crowded region of the sky — the DSS2 red survey shows there are at least 10 sources in the XRT extraction radius, so source confusion cannot be ruled out. To test how this may affect the light-curve decay parameters we included a constant component to the model and found they are consistent with the values quoted above, with $\alpha_1 = 5.05^{+0.55}_{-0.40}$, $t_b = 258^{+30}_{-20}$ s, $\alpha_2 = 1.06^{+0.15}_{-0.13}$ and a constant level of $2.5^{+0.15}_{-0.10} \times 10^{-4}$ counts s^{-1} ($\chi^2/\nu = 12.2/17$).

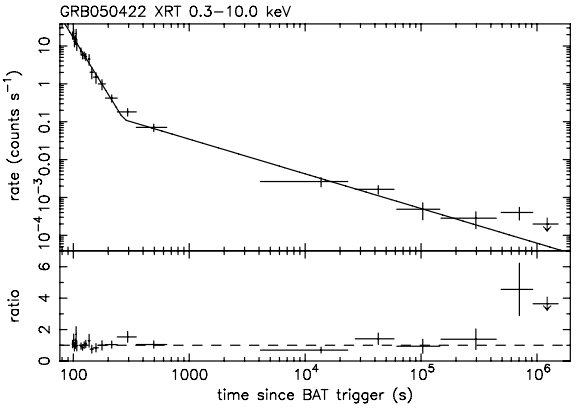

Figure 3. The XRT light curve from GRB 050422 covering the energy range 0.3–10.0 keV, plotted with respect to the BAT trigger time. The data are modelled with a broken power-law decay curve.

The broken power-law fits to the light curve were made assuming the BAT trigger time represents the onset of the X-ray emission. The main gamma-ray peak, however, starts at $T + 45$ s and could alternatively be associated with the start of the X-ray emission. Shifting the zero time of the fit by this amount alters the X-ray decay parameters to $\alpha_1 = 3.22^{+0.45}_{-0.25}$, $t_b = 281^{+90}_{-84}$ s, $\alpha_2 = 0.85^{+0.14}_{-0.13}$, ($\chi^2/\nu = 13.0/18$).

Using the best-fitting spectral model discussed below, the unabsorbed 0.3−10.0 keV fluxes at 1 and 10 h were estimated to be 1.0×10^{-12} and 1.3×10^{-13} erg cm^{-2} s^{-1}, respectively. GRB 050422 is one of the faintest GRBs observed by the XRT one hour after the initial trigger (Nousek et al. 2006; O'Brien et al. 2006; Roming et al. 2006).

2.2.2 *Spectral analysis*

Spectra in WT and PC mode were extracted using the same analysis techniques described above, and the early PC data were corrected for the pile-up. A detailed spectral analysis was hampered by the limited statistics. The WT (grade 0–2, exposure 18 s) and PC (grade 0–12) spectra for the first observation segment were jointly fit with a model consisting of an absorbed power law. Allowing the absorption to vary in the fit produced an upper limit of 1.5×10^{22} cm^{-2} on the column density to this source. In the remainder of the analysis, the column was fixed at the Galactic value of 1×10^{22} cm^{-2} (Dickey & Lockman 1990). The best-fitting WT and PC mode spectral indices were found to be $\beta_X = 2.33^{+0.58}_{-0.55}$ and $1.65^{+0.59}_{-0.50}$, respectively, with $\chi^2/\nu = 3.0/7$.

The early-time XRT spectrum is much softer than that inferred by the BAT, as illustrated by the residuals in Fig. 2. Such a hard-to-soft evolution trend is not unusual in the context of GRB prompt emission, and has also been seen in BATSE observations of long bursts (Bhat et al. 1994; Ford et al. 1995; Crider et al. 1997). Ryde & Petrosian (2002) showed it is possible to produce such spectral softening providing the curvature of the relativistically expanding shell is taken into account, even when the intrinsic spectrum is unchanged.

The PC spectrum discussed above includes both pre- and post-break emission. An attempt was made to divide the data from the first segment at the break to search for possible spectral variations. However, the fits were poorly constrained giving pre- and post-break β_X values of 1.9 ± 0.5 ($\chi^2/\nu = 5.1/4$) and $1.0^{+1.0}_{-0.9}$ ($\chi^2/\nu = 2.22/3$), respectively. Likewise, data from segments two ($T + 4.1$ ks) to five ($T + 445$ ks) combined gave $\beta_X = 1.4^{+1.3}_{-0.9}$. There are consistent hints that the spectrum hardens during the XRT observation, although the measured changes are within the formal errors.

2.3 Optical

The UVOT telescope is co-aligned with the XRT, and it began observing the burst at the same time. However, only 5σ upper limits of 17.8 (U), 18.2 (B), and 17.9 (V) were obtained to any prompt optical emission (occurring at mid-times of 418, 432 and 374 s, respectively) from this burst (McGowan et al. 2005). The source was located close to the Galactic plane with a reddening in its direction of $E_{B-V} = 1.4$ (Schlegel, Finkbeiner & Davis 1998). No ground-based follow-up observations were reported.

3 DISCUSSION

The most complete sample of *Swift* GRBs published thus far can be found in O'Brien et al. (2006). For the 39 long GRBs presented there, we find bursts which are promptly followed-up by the XRT have mean parameters $\langle\beta_B\rangle = 0.74$, $\langle\beta_X\rangle = 1.13$ and $\langle\alpha_1\rangle = 2.38$, with corresponding standard deviations of 0.51, 0.75 and 1.50, respectively. Therefore, while GRB 050422 has a BAT spectral index comparable to other bursts, it has one of the steepest early declines seen in the X-ray data (1.8σ deviation from the mean), along with a softer than average spectrum (1.6σ from the mean), whereas the post-break temporal decay is consistent with other bursts. In fact, only GRB 050714B has more extreme temporal decay and spectral indices at early times (Levan et al., in preparation), while GRBs 050315, 050803, 050819 and 050915B have comparably steep temporal decays, and GRBs 050126, 050315, 050319 and 050908 have spectra consistent with being as soft, though some have large associated uncertainties (Nousek et al. 2006; O'Brien et al. 2006).

3.1 The initial steeply declining light curve

Evidence is mounting that the rapidly declining X-ray light curves observed by *Swift* are linked to the prompt gamma-ray emission, while the later, slow decline, corresponds to the familiar GRB afterglow (see Nousek et al. 2006; O'Brien et al. 2006; Zhang et al. 2006).

Fig. 4 shows the combined BAT/XRT light curve for GRB 050422 where the observed count rate in each instrument has been renormalized to an unabsorbed flux in the 0.3–10.0 keV XRT band following the method of O'Brien et al. (2006). To account for the spectral curvature seen between the BAT and XRT observations, the mean BAT–XRT spectral slope, $\beta_{mean} = 1.4$, was used in the BAT conversion, while the measured $\beta_X = 2.3$ was used for the XRT. The figure illustrates that the early XRT light curve joins up well with the late time BAT data, and that the flux drops by four orders of magnitude in just ∼250 s. The steeply declining early X-ray emission, therefore, appears to be associated with the tail of the prompt gamma-ray emission rather than the conventional, forward-shock-created, afterglow.

Indeed, for the standard afterglow models summarized in table 1 of Zhang & Mészáros (2004), the data from before the light curve break either fail to comply with the α, β relations or require too high a value for p (the power-law distribution of relativistic electron energies). For example, the standard ISM model (Sari, Piran & Narayan 1998; Zhang & Mészáros 2004), predicts $\alpha_X = (3\beta_X - 1)/2$ if the

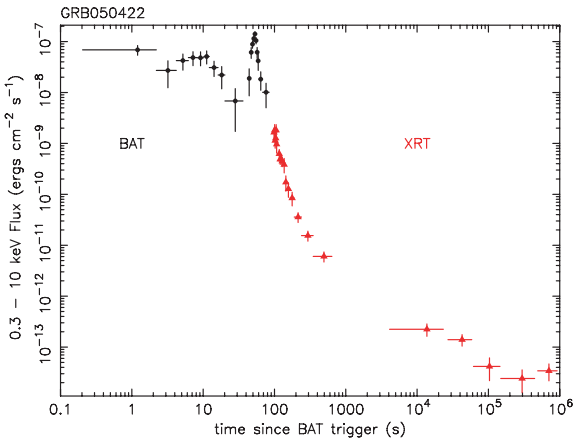

Figure 4. BAT (circles) and XRT (triangles) light curves normalized to 0.3–10.0 keV unabsorbed fluxes, showing that the late-time BAT and early XRT decay join up.

observed frequency $\nu > \max(\nu_m, \nu_c)$, where ν_m is the synchrotron injection frequency and ν_c is the cooling frequency, or $\alpha_X = 3\beta_X/2$ if $\nu_m < \nu < \nu_c$. The measured value of $\beta_X \approx 2.3$ gives $\alpha_X \approx 3.0$ or 3.5 for these models, respectively, which are inconsistent with the observed value of α_X at early times. In both cases, the implied value of the electron energy distribution, as obtained from β_X, is $p \sim 4.4-5.6$, which is much higher than the 'universal' value of $p \sim 2.2$. Recently, Shen, Kumar & Robinson (2006) have questioned the universality of p, and have shown that the standard deviation of its distribution, as obtained from BATSE bursts, is $\sim$0.5. Even so, the value estimated above would be an extreme outlier to this distribution ($\sim 4\sigma$) and thus unlikely, further emphasizing the inadequacy of the standard forward-shock models when applied to the early X-ray data.

A possible explanation for the steeply falling light curve at the end of the prompt emission phase exists in the form of the high-latitude emission model of Kumar & Panaitescu (2000). In this scenario, if a shell of material abruptly stops radiating, the observer encounters delayed emission from progressively larger angles, θ, to the line of sight, provided $\theta \gg \Gamma^{-1}$ (where Γ is the bulk Lorentz factor of the jet). The model predicts a steeply decaying flux with $\alpha = \beta + 2$. Also, the spectrum shifts to lower frequencies as the emission from higher latitudes has smaller Doppler boost factors (Zhang et al. 2006). The measured β_X at early times, therefore, suggests α should lie in the range from 3.8 to 4.9 if emission from high latitudes is seen. This is satisfied by the observed values provided the zero time for the X-ray emission is taken to be the BAT trigger time. However, with such a well-defined late pulse seen in the BAT data, we really expect the zero time to be taken as the onset of this peak, as implied by the smoothly joining light curve of Fig. 4. In this case, the observed $\alpha \sim 3.2$ is slightly flatter than the $\beta + 2$ prediction.

Zhang et al. (2006) have discussed how departures from the $\alpha = \beta + 2$ relation could arise. In particular, a shallower α would be expected if emission from the forward shock is already contributing. In an attempt to account for this, we have propagated the post-break power-law decay back to early times and subtracted its contribution from the pre-break light curve. This steepens the pre-break decay index to $3.6^{+0.4}_{-0.3}$, which can once more be accounted for by the prediction of the high-latitude model within the uncertainties.

The observed differences in the BAT and XRT spectral indices, and the fact that we see a smooth transition in the combined light curve (Fig. 4) using the mean BAT–XRT spectral index of $\beta_{mean} = 1.4$, suggests there could be spectral curvature between the BAT and XRT bands. If this is the case then the appropriate value for β in the $\alpha = \beta + 2$ relation would also be the mean spectral index, which in turn would give rise to a shallower decay slope of $\sim$3.4, again, consistent with that obtained from the data when the forward-shock contribution is taken into account. Such spectral curvature is not unexpected in the framework of the high-latitude emission model: as the decay progresses we expect to see emission from higher and higher latitudes but with correspondingly smaller Doppler shifts. The XRT band therefore receives emission from larger comoving frequencies, i.e. approaching the comoving frequency of the BAT band.

The $\alpha = \beta + 2$ relation is only valid for frequencies above the cooling frequency when there is no radiation from on-axis elements. If the cooling frequency of any on-axis emission was situated in the XRT band, then, even after the shock crossing, the on-axis shell element would radiate photons at frequencies lower than the cooling frequency. Any contribution from the on-axis element would enhance the low-frequency emission which could result in a steeper spectrum when the on- and off-axis emissions are both taken into account. This could account for the steep spectral index observed at early times by the XRT and also produce a shallower decay slope.

Alternatively, the observed α may be shallower than the $\alpha = \beta + 2$ relation if the shell responsible for the emission radiates continuously, or if there is a hidden small peak in the tail of the decay.

The observed flux from high-latitude emission in the rest frame of the burst is expected to fall off rapidly on a time-scale $t > \delta t(\Gamma\theta_\circ)^2$ (Kumar & Panaitescu 2000), where δt is the duration of the emitting pulse, Γ is the Lorentz factor of the outflow, and $\theta_\circ$ is its opening angle. If $\delta t \sim 10$ s, as measured by the duration of the main-peak in the BAT emission, and Γ is typically $\sim$100, then an angular size for the outflow of $\theta_\circ \sim 4^\circ$ is sufficient for the emission to have decayed in $\sim$500 s as implied by the foward-shock subtracted X-ray light curve. We might ask if the estimated opening angle is consistent with the lack of an observed jet-break in X-ray light curve. The typical Frail et al. (2001) parameters would imply an opening angle $\gtrsim 8^\circ$ if the jet-break occurred later than $\sim$10 d after the trigger. This could easily be reconciled with the opening angle derived from the high-latitude emission model if the burst parameters were atypical; in particular, a low density ambient medium ($\lesssim 0.1$ cm^{-3}) would have the desired effect, and would also be consistent with the faintness of the afterglow seen at later times. However, we note Sato et al. (2006) has presented evidence of three *Swift* bursts with redshift determinations which, although they follow the expected spectral peak energy/isotropic energy release of the Amati et al. (2002) relation, show no sign of a jet-break at the predicted times. This suggests jet-breaks are not necessarily ubiquitous in X-ray light curves.

3.2 Post-break light curve

The post-break temporal decay of $\alpha_2 \approx 0.9$ is entirely consistent with the emergence of the normal X-ray afterglow, once the prompt emission has died away. The temporal and spectral properties of the afterglow depend on the assumed density profile of the surrounding environment. Both the standard ISM and wind models can account for the observed decay index with $p \sim 2.0$–2.2. However, the large uncertainty in the post-break spectral index means we are unable to distinguish between these models. The fact that the X-ray light curve is always declining throughout the transition from the prompt emission to the afterglow suggests that the afterglow is already established by the time of the break, $\sim$270 s after the gamma-ray burst began.

The X-ray flux in the afterglow is unusually low one hour after the burst trigger. Of the long bursts in O'Brien et al. (2006), only GRBs 050412 and 050421 are fainter at this stage of the outburst. This makes GRB 050422 appears to be a gamma-ray efficient burst. One explanation for the weakness of the afterglow is it could simply be indicative of a low-density circumburst environment. The lack of significant optical emission would be due to the high Galactic extinction in the direction of the burst (Roming et al. 2006).

4 CONCLUSIONS

Swift observations of the long gamma-ray burst GRB 050422 have been presented. In the 15−150 keV gamma-ray band, the burst had a T_{90} duration of 59 s and exhibited a multipeaked light curve, with the main event occurring 53 s after the initial trigger. X-ray observations began within 100 s of the trigger and showed an initially steeply declining 0.3–10.0 keV light curve which flattened after $\sim$270 s and could be fitted by a broken power-law decay. The measured X-ray decay parameters depend on the choice of zero time: using

the BAT trigger time as the zero-point gives a pre-break index $\alpha_1 = 4.97^{+0.53}_{-0.37}$, a break time $t_b = 272^{+43}_{-25}$ s and a post-break index $\alpha_2 = 0.92^{+0.13}_{-0.16}$, whereas allowing the zero time to coincide with the onset of the main peak in the gamma-ray light curve gives $\alpha_1 = 3.22^{+0.45}_{-0.25}$, $t_b = 281^{+90}_{-84}$ s and $\alpha_2 = 0.85^{+0.14}_{-0.13}$. The initial decline is steep either way.

The X-ray spectrum at $T + 124$ s was also steep, with an energy index $\beta_X = 2.33^{+0.58}_{-0.55}$. No discernible spectral variations were observed at later times.

The 0.3–10.0 keV flux normalized BAT/XRT light curve show that the early time X-ray emission joins up well with the late time gamma-ray emission, indicating that the initial XRT measurements were made during the tail of the prompt emission. The steep temporal index of the prompt emission can be explained with the high-latitude emission model, while the shallower post-break decay is consistent with a standard, though faint, afterglow.

ACKNOWLEDGMENTS

This work is supported at the University of Leicester by the Particle Physics and Astronomy Research Council (PPARC), and at the ASDC by the Italian Space Agency (ASI). We thank the referee for comments which helped to improve the clarity of this paper.

REFERENCES

Amati L. et al., 2002, A&A, 390, 81
Barbier L., Palmer D., Burrows D. N., Blustin A., Krimm H., Gehrels N., McGowan K., Chester M., 2006, GCN, 3314
Barthelmy S. D. et al., 2005, Sp. Sc. Rev., 120, 143
Bhat P. N., Fishman G. J., Meegan C. A., Wilson R. B., Kouveliotou C., Paciesas W. S., Pendleton G. N., Schaefer B. E., 1994, ApJ, 426, 604
Bloom J. S., Frail D. A., Kulkarni S. R., 2003, ApJ, 594, 674
Burrows D. N. et al., 2005a, Sp. Sc. Rev., 120, 165
Burrows D. N. et al., 2005b, Sci, 309, 1833
Crider A. et al., 1997, ApJ, 479, L39
Cusumano G. et al., 2006, ApJ, 639, 316
Dickey J. M., Lockman F. J., 1990, ARA&A, 28, 215
Falcone A. et al., 2006, ApJ, 641, 1010
Ford L. A. et al., 1995, ApJ, 439, 307
Frail D. A. et al., 2001, ApJ, 562, L55
Frontera F., 2003, Lec. Notes Phys., 598, 317
Gehrels N. et al., 2004, ApJ, 611, 1005
Goad M. R. et al., 2006, A&A, 449, 89
Hill J. E. et al., 2004, SPIE, 5165, 217
Hjorth J. et al., 2003, Nat, 423, 847
Kumar P., Panaitescu A., 2000, ApJ, 541, L51
MacFadyen A. I., Woosley S. E., 1999, ApJ, 524, 262
McGowan K. et al., 2005, GCN, 3317
Mészáros P., Rees M. J., 1997, ApJ, 476, 232
Moretti A. et al., 2004, SPIE, 5165, 232
Moretti A. et al., 2006, A&A, 448, L9
Nousek J. A. et al., 2006, ApJ, 642, 389
O'Brien P. T. et al., 2006, ApJ, 647, 1213
Piro L., 2004, in Feroci M., Frontera F., Masetti N., Piro L., eds, ASP Conf. Ser. Vol. 312, Third Rome Workshop on Gamma-Ray Bursts in the Afterglow Era. Astron. Soc. Pac., San Francisco, p. 149
Rees M. J., Mészáros P., 1994, ApJ, 430, L93
Romano P. et al., 2006, A&A, 450, 59
Roming P. W. A. et al., 2005, Space Sci. Rev., 120, 95
Roming P. W. A. et al., 2006, ApJ, 652, 1416
Ryde F., Petrosian V., 2002, ApJ, 578, 290
Sari R., Piran T., Narayan R., 1998, ApJ, 497, L17
Sato G. et al. 2006, ApJ, in press
Schlegel D. J., Finkbeiner D. P., Davis M., 1998, ApJ, 500, 525
Shen R., Kumar P., Robinson E. L., 2006, MNRAS, 371, 1441
Stanek K. Z. et al., 2003, ApJ, 591, L17
Suzuki M. et al., 2005, GCN, 3316
Tagliaferri G. et al., 2005, Nat, 436, 985
Vaughan S. et al., 2006, ApJ, 638, 920
Woosley S. E., 1993, ApJ, 405, 273
Zhang B., Mészáros P., 2004, Int. J. Mod. Phys, 19, 2385
Zhang B., Zhong Fan Y., Dyks J., Kobayashi S., Mészáros P., Burrows D. N., Nousek J. A., Gehrels N., 2006, ApJ, 642, 354
Zhang W., Woosley S. E., Heger A., 2004, ApJ, 608, 365

This paper has been typeset from a TEX/LATEX file prepared by the author.